Refractivity Retrieval Using the Phased-Array Radar: First Results and Potential for Multimission Operation

Boon Leng Cheong, Robert D. Palmer, Christopher D. Curtis, Tian-You Yu, Dusan S. Zrnić, and Douglas Forsyth

***Abstract*—In this paper, an investigation of the potential of rapid refractivity retrieval is presented. The retrieval technique utilizes radar phase measurements of ground clutter to derive near-surface refractivity, which has been commonly used as a proxy for humidity, given its close relation to vapor pressure. Surface humidity is an important meteorological parameter and has been known to play an important role in convective initiation. In this paper, the refractivity retrieval technique is exploited by using smaller numbers of samples for phase calculation, which is a fundamental process in refractivity retrieval. The impetus for this paper is to explore the possibility of rapid refractivity retrieval by exploiting the rapid beam-steering capability of a phased-array radar. Using the National Weather Radar Testbed in Norman, OK, a 64-pulse per radial raw-data set was collected for conventional refractivity processing. Then, subsets of the 64 samples were extracted to emulate shorter dwell periods and the corresponding more rapid experiments. The test cases that were considered are 2, 4, 8, 16, and 32 samples. Refractivity fields retrieved using smaller numbers of samples are compared against the reference field, which was obtained using the entire 64-sample data set. It will be shown that, statistically, significant refractivity fields can be obtained from as short as a two-sample dwell.**

***Index Terms*—Array signal processing, meteorological radar, phased array radar, rapid refractivity retrieval, surface refractivity.**

I. Introduction

SINCE near-surface refractivity has become feasible to be retrieved remotely from convectional weather radars [1], [2], the refractivity retrieval technique has received increasing attention from the meteorological community due to the close relation between refractivity and the atmospheric vapor pressure. Surface refractivity can play an important role in weather forecasting. In fact, it has been reported that parameterization of surface moisture is one of the crucial components for accurate prediction of convective initiation (e.g., [3] and [4]). In addition, results from numerical modeling have shown that the intensity of convective-precipitation systems is sensitive to the surface moisture [5]. Therefore, it is desirable and potentially viable to assimilate high-resolution surface refractivity into forecasting models, but this activity is limited at the present time. Radiosonde launches do not provide sufficient spatial or temporal resolution, particularly in environments with convective rolls, in which the twice-daily measurement is simply not representative [6]. Besides convective scale forecasting/modeling, surface-refractivity measurement also plays an important role for mesoscale applications. It has been shown that large horizontal variations in moisture, such as drylines, are related to initiation of deep convection (e.g., [7]–[9]). In the work of Guo *et al.* [10], a rather counterintuitive result was reported in which the surface dew point temperature (closely related to surface refractivity) was found to have significant influence on the recovery of the vertical moisture profile in 4-D variational data assimilation system. The recovery of the vertical profile is important for extended runs of the model.

In the first work of its kind, Fabry *et al.* [1] successfully used phase measurements from ground clutter to derive refractivity fields within the regions with sufficient stationary ground targets using an S-band weather radar. This technique has been refined over the years, and a more recent description of the technique can be found in [2]. During the International H_2O Project (IHOP_2002), [11] deployed in the Southern Great Plains of the U.S., extensive experiments of refractivity retrieval were conducted, and it was shown that the refractivity fields measured using this technique are in good agreement with surface measurements. Based on this paper, an independent processing algorithm for refractivity retrieval has been developed here at the University of Oklahoma (OU), and its application to phased-array radar is the focus of this paper [12].

As mentioned earlier, refractivity retrieval from phase measurement relies on radar echoes from ground targets and, thus, is susceptible to earth curvature. In nonmountainous regions, ground targets are typically detected up to 40–50 km, and therefore, the refractivity field can be derived within this range. Recently, a closely spaced radar network has been proposed by the NSF ERC Collaborative Adaptive Sensing of the Atmosphere (CASA), [13] for observations of low-altitude

Manuscript received August 2, 2007; revised December 20, 2007. This work was supported in part by the NOAA National Severe Storms Laboratory under Cooperative Agreement NA17RJ1227.

B. L. Cheong and R. D. Palmer are with the School of Meteorology, University of Oklahoma, Norman, OK 73072 USA (e-mail: boonleng@ou.edu).

C. D. Curtis is with the National Severe Storms Laboratory, National Oceanic and Atmospheric Administrations (NOAA)/OAR, Norman, OK 73072 USA, and also with the Cooperative Institute of Mesoscale Meteorological Studies, University of Oklahoma, Norman, OK 73072-7304 USA.

T.-Y. Yu is with the School of Electrical and Computer Engineering, University of Oklahoma, Norman, OK 73072 USA.

D. S. Zrnić and D. Forsyth are with the National Severe Storms Laboratory, National Oceanic and Atmospheric Administrations (NOAA)/OAR, Norman, OK 73072 USA.

Color versions of one or more of the figures in this paper are available online at http://ieeexplore.ieee.org.

Digital Object Identifier 10.1109/TGRS.2008.919506

weather phenomena. The goal of the concept system is to observe the lower portions of the atmosphere, which are usually not covered by the existing WSR-88D radar network due to earth curvature. Here in Oklahoma, a testbed with a network of four X-band radars has been implemented by the CASA effort. The radar separation for this network is targeted approximately 30 km and, hence, would mitigate the Earth curvature limitation on the observation of ground targets. Studies are currently being conducted at OU for refractivity retrieval using these X-band radars [14], [15].

In this paper, the concept of rapid refractivity retrieval is investigated through the use of electronic scanning provided by the National Weather Radar Testbed–Phased-Array Radar (NWRT PAR), which is operated by the National Severe Storms Laboratory (NSSL) [16]. The agile beam-steering capability of the NWRT PAR was exploited to investigate the feasibility of deriving refractivity with an extremely small numbers of samples. Dwell times, as short as 180 ms for a 90° coverage, are tested, and the results will be presented here. A Multimission PAR (MPAR, also known as the multifunction PAR) concept has been proposed, in which a PAR simultaneously performs a number of tasks, such as weather observations and aircraft tracking, by exploiting the fast beam-steering capability [17]. If the MPAR system is to become a reality, rapid acquisition of refractivity fields would be an attractive component of the system. It should be made clear at this point that the core of the refractivity retrieval technique is to obtain the refractivity change, i.e., not an absolute quantity. In practice, however, this drawback can be circumvented by strategically applying the technique. In the approach of [2], a reference refractivity field that is spatially homogeneous at a given time with the associated phase field is first obtained, and all the subsequent refractivity change fields, retrieved from radar, are added to this reference field to obtain the absolute refractivity. The approach can be easily implemented and has been shown to be robust [2]. Nonetheless, in the scope of this paper, the goal is to investigate the core technique itself, and therefore, we will focus on the refractivity change for quantitative evaluation and discussion throughout this paper.

The remainder of this paper is organized as follows. A brief overview of the PAR system will be presented in Section II. A summary of OU's refractivity retrieval algorithm will be presented in Section III. Experimental results will be provided in Section IV, followed by discussions of rapid refractivity retrieval in the MPAR system design in Section V, and the conclusions are presented in Section VI.

II. Brief Overview of the PAR

The AN/SPY-1A PAR system has been used effectively for years on the Navy's Aegis-class missile guidance systems [18]. Under the auspices of a multiagency project, including government, private industry, and university groups, the SPY-1A phased-array antenna has been adapted for meteorological research under the direction of the NSSL [19]. This advanced weather radar is referred to as the PAR and is the main instrument of the NWRT located in Norman, OK [16]. The PAR utilizes a WSR-88D transmitter, modified to operate at 3.2 GHz. Both transmit and receive operations are handled by the antenna, which is an array of 4352 elements. Real-time beamforming is used to electronically steer the beam over the desired volume coverage pattern. The data acquisition system allows the storage of raw time-series data for up to 24 h of continuous operation. Obviously, the most attractive feature of the PAR system is its agile beam-steering capability, which allows complete flexibility in pointing direction from pulse-to-pulse within $\pm 45^\circ$ of broadside. As a result, beam-smearing effects, that are inherent in standard scanning radars such as the WSR-88D due to antenna motion, are eliminated in the PAR system. In addition, it supports adaptable scanning strategies and volumetric scans of a storm on time scales of seconds instead of several minutes [19]. This capability enables the study of rapidly evolving weather phenomena, which may potentially improve warning lead-time for severe weather.

Fig. 1. Photograph of the NWRT PAR system during radome installation. The antenna array is housed inside the dome at approximately 12 m above the ground.

A photo of the NWRT PAR is shown in Fig. 1. The three-story building houses the array antenna on the top floor, approximately 12 m above the ground, covered with a fiberglass dome. Real-time data-processing units and data acquisition equipment are housed on the second floor of the building. The bottom floor stores maintenance tools and test apparatus. During operations, the PAR can be controlled remotely without the need of human intervention in this building, and the radar products are sent to NSSL via a conventional computer network. An artistic depiction of the PAR concept is shown in Fig. 2. Due to the effective aperture for different look directions, the beamwidth is 1.5° at broadside and 2.1° at 45° off broadside.

III. Summary of OU's Refractivity Retrieval Algorithm

Based on the work by Fabry [2], an independent processing algorithm for the retrieval of refractivity fields from ground-clutter signals has been developed at OU. Here, we will outline the fundamental concepts of the technique, highlighting the differences from the original algorithm. In theory, the signal phase from a stationary target is an integral function of the refractive index, which can be retrieved by performing a range derivative operation. In practice, however, the typical radar wavelength is on the order of centimeters, and the refractive

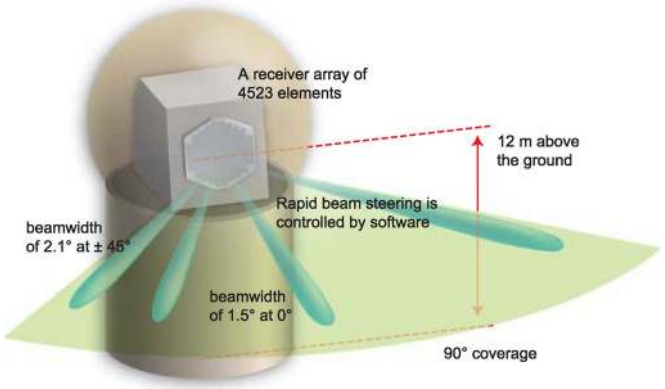

Fig. 2. Artistic depiction of the PAR. Due to the effective aperture for different look directions, the beamwidth is 1.5° at broadside and 2.1° at 45° off broadside. Using electronic scanning, the beam can be steered rapidly from one position to another. Here, this agile beam-steering capability is exploited for rapid refractivity retrieval.

index is near unity, so the phase wraps thousands of times within a resolution volume depth, making the retrieval process impossible. To mitigate this phase-wrapping problem, Fabry [2] proposed that the processing be performed on the change of signal phase between two scans. By doing so, phase wrapping is significantly reduced, and refractivity retrieval is made possible. If the absolute refractivity field of one of the scans is known, for example, by surface measurements, the refractivity change allows the estimation of absolute refractivity by simply adding the difference to the known field.

In the following sections, the relationship between refractivity and signal phase is reviewed, OU's refractivity retrieval algorithm is provided, and several practical implementation issues are examined. It is worth mentioning that such details were not found in the literature but based on our development experience, the following approach provides a robust and efficient retrieval algorithm.

A. Signal Phase: The Fundamental Quantity for Refractivity Retrieval

Refractive index n of a medium is defined as the ratio of the speed of light in a vacuum to the speed of light in the medium. For air near the surface of the Earth, $n \approx 1.003$, and changes of this number are on the order of 10^{-5}. For numerical convenience, a derived quantity, referred to as refractivity, is often used and is described as follows [20]:

$$N = 10^6(n-1). \tag{1}$$

It can be shown that refractivity is related to meteorological parameters as provided in the following [20]:

$$N = 77.6\frac{p}{T} + 3.73 \times 10^5 \frac{e}{T^2} \tag{2}$$

where p represents the air pressure in hectopascals, T is the absolute air temperature in kelvin, and e represents the vapor pressure in hectopascals. The first term in (2) is proportional to pressure p and is, therefore, related to the air density. The second term is proportional to vapor pressure e, which is

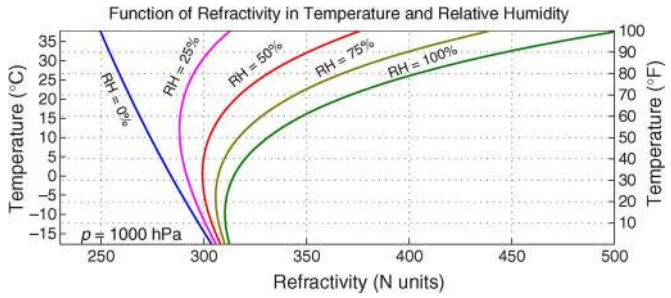

Fig. 3. Refractivity N as a function of temperature T and relative humidity (derived from T and e). At a surface pressure of 1000 hPa and temperature above 10 °C, refractivity changes are predominantly affected by the relative humidity (vapor pressure).

directly related to atmospheric moisture. The two terms are often referred to as the dry and wet terms, respectively. Near the surface of the Earth and in relatively warm temperatures, the spatial variability in N is dominated by changes in the second term. To illustrate this point, refractivity is shown in Fig. 3 as a function of temperature for a range of relative humidity values. As temperature increases, N becomes more sensitive to changes in e and, thus, can be used as a proxy for water vapor near the surface. For temperatures below freezing, the refractivity has significantly smaller variations due to both temperature and moisture. As a result, radar-based refractivity retrieval may be more applicable during warm-season events.

By definition of the refractivity index, the time needed for an electromagnetic wave to travel the two-way path between the radar and a target at range r is given by the following:

$$t_{\text{travel}} = 2r\frac{n}{c} \tag{3}$$

where c is the speed of light in a vacuum (299 792 458 m $\cdot$ s^{-1}). This travel time is measured by a weather radar by the delay of the transmit pulse. However, the accuracy of such a measurement does not allow the estimation of subtle changes in refractive index. Accuracies of this scale must be made using the signal phase, which is described as follows:

$$\phi(r) = -2\pi f t_{\text{travel}} = -\frac{4\pi f}{c}\int_0^r n(\gamma)d\gamma \tag{4}$$

where f is the transmitted frequency of the radar. Note that the radar phase is proportional to the path-integrated refractive index. As mentioned before, the phase will wrap approximately every half a wavelength, as can be seen from the multiplicative term in front of the integral.

Four examples from the PAR of phase measurements of ground targets are shown in Fig. 4. The measurements were taken over a 1-h period and are from targets at ranges of 14.3, 14.7, 15.2, and 15.7 km. It is first noticed that there is a general trend of increasing phase from ground targets using the PAR. The phase measurement was collected for an hour, and during this period, there was a decreasing trend in n (from surface measurements) so we expect an increase in the phase measurement [refer to (4)]. For stationary ground targets, one can see slow variation in phase due to the change of N. For

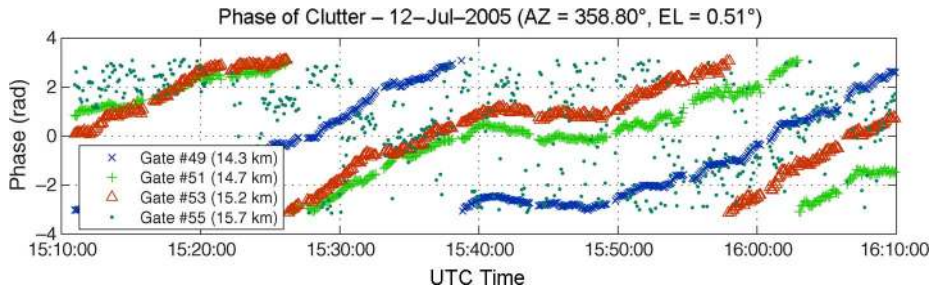

Fig. 4. Temporal phase variation from four ground targets. Three sets of slowly varying phase indicate the phase change due to refractivity change. These targets are stationary, so they are suitable for refractivity retrieval. These targets were chosen here because of their high reflectivity and zero Doppler velocity, which provide good SNR and stationary phase. Another phase that appears random is most likely from a nonstationary target and, therefore, cannot be used for refractivity retrieval.

nonstationary ground targets (fading), such as that at 15.7 km, the phase measurement exhibits a high statistical variation, thus should not be used for refractivity retrieval. Such fading ground targets are normally excluded from the processing scheme, as will be emphasized later.

B. Algorithmic Flow and Imaging Processing Procedures

The fundamentals of radar-based refractivity retrieval can be found in [1] and [2]. For the sake of completeness, it is briefly reviewed in this section. As mentioned earlier, unwrapping the phase is problematic due to the short wavelength relative to the range resolution depth. To circumvent this limitation, Fabry *et al.* [1] proposed that the processing be performed on the phase change between two scans instead of the phase from a single scan. This calculation is given by the following:

$$\begin{aligned}\Delta\phi(r) &= \phi(r,t_1) - \phi(r,t_0) \\ &= -\frac{4\pi f}{c}\int_0^r [n(\gamma,t_1) - n(\gamma,t_0)]\,d\gamma \end{aligned} \tag{5}$$

where t_1 and t_0 correspond to the two scan times. From this equation, one can see that the change of phase is a function of the integrated change of refractive index. By applying a range derivative operator to (5), it can be shown that

$$\frac{d}{dr}[\phi(r,t_1) - \phi(r,t_0)] = -\frac{4\pi f}{c}[n(r,t_1) - n(r,t_0)]. \tag{6}$$

Usually, measurement at time t_0 is referred to as the reference, with $n(r,t_0)$ being the reference refractive index. From the right-hand side of (6), one can see that the derivative of the phase difference is directly proportional to the refractive-index difference. Therefore, refractivity difference ΔN can be derived by performing a radial derivative on the phase difference field

$$\begin{aligned}\Delta N &= -10^6\,[n(r,t_1) - n(r,t_0)] \\ &= -10^6\frac{c}{4\pi f}\frac{d}{dr}[\phi(r,t_1) - \phi(r,t_0)]. \end{aligned} \tag{7}$$

A flowchart of the refractivity retrieval algorithm is shown in Fig. 5. Each step will be discussed in the following sections. As one can see from the top of the figure, the first step is to calculate the so-called phase difference map. Some phase

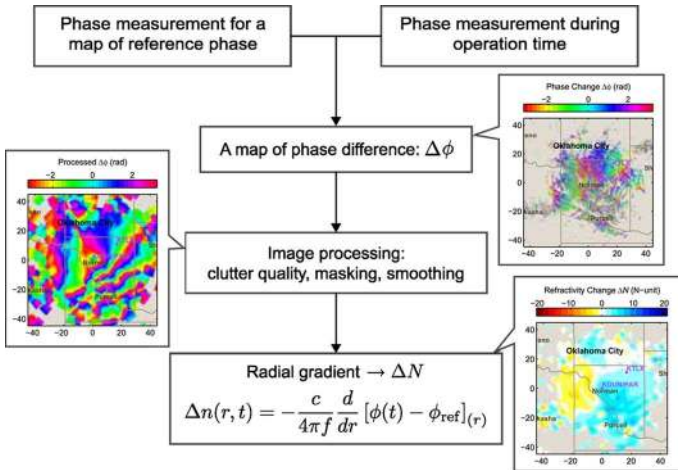

Fig. 5. Procedure of refractivity retrieval. Two fields of phase measurement are needed for each retrieval. A so-called phase difference map is derived from these two fields of measurements and subsequently masked for areas that are usable. The masked phase difference map is shown on the right-hand side of the flowchart. Then, imaging processing is performed to obtain a smooth and continuous map (shown in the upper left panel). Finally, a range derivative is computed on a gate-by-gate basis. The range derivative is scaled appropriately to obtain the change of refractive index (or refractivity).

measurements (from poor-quality targets) cannot be used and are disregarded in a process referred to as masking.

1) Phase Difference Calculation and Masking: For the raw phase difference calculation, the reference phase map is subtracted from the measurement phase map on a gate-by-gate basis. Each value is then modulo-mapped into $[-\pi, +\pi]$. Usable phase values are kept (masked in) if they are associated with targets that are quality ground-clutter targets, i.e., have high signal-to-noise ratio (SNR), near-zero radial velocity (v_r), and narrow spectral width (σ_v). Otherwise, the phase values are set to zero (masked out). Subsequently, this map is filtered with a 2-D Gaussian window to achieve smoothing and interpolation. The process is similar to an up-sampling procedure in which zeroes are first inserted in between samples then fed into a low-pass filter for interpolation. The complete masking procedure is based on two distinct qualities, i.e., the reliability index (RI) and the quality index (QI), both of which will be described as follows.

The RI is a measure of the variability of the measured phase, typically over at least an hour time period. If the observed moisture field does not change significantly over this 1-h period, the phase should be approximately constant. A measure of

this variability is given by the RI, which is calculated with the following [1]:

$$\mathrm{RI} = \frac{1}{M}\left|\sum_{n=0}^{M-1}\exp(j\phi[n])\exp(-j\phi[n-L])\right| \tag{8}$$

where n corresponds to the scan number, M represents the total number of realizations, and L is the scan lag, which is typically taken as one scan. If the refractivity is constant, the phase should also be constant and would result in RI ≈ 1 for stationary targets. Vibrations in clutter targets (fading) cause a reduction in the value of RI. One may consider an advantage of using $L > 1$ to measure RI for higher lags, but in general, an L factor of at least 5-min is adequate. In practice, a completely constant refractivity field of over an hour is extremely difficult to obtain. Therefore, one need to choose a value that is lower than 1.0 when deriving RI under quasi-homogeneous conditions. In our experience, when refractivity is varying slowly over the hour, i.e., < 5 N unit, an RI threshold of 0.7 provides a good separation between usable and nonusable targets.

The QI is a measure of the quality of fixed targets, based on the spectral characteristics of the target, and is mathematically described as follows (Fabry, personal communication):

$$\mathrm{QI} = \frac{1}{1+10^{-0.1\,\mathrm{SNR}}}\exp\left[-\left|\frac{v_r}{v_t}\right|^4\right]\exp\left[-\left(\frac{\sigma_v}{\sigma_t}\right)^4\right] \tag{9}$$

where v_t and σ_t are the masking thresholds for radial velocity and spectral width, respectively. Typical values of v_t and σ_t are 0.5 and 5 $\mathrm{m}\cdot\mathrm{s}^{-1}$, respectively. Masking through QI can be thought of as a process to eliminate weather contamination by rain. However, there are still instances in which it fails to mitigate the weather interference. This usually occurs at the direction in which the weather is moving slowly, i.e., within the Doppler velocity threshold, or is perpendicular to the beam-pointing direction, which results in zero Doppler velocity. Nonetheless, refractivity measurements are mostly interested during clear conditions. For positions with RI < 0.7 and QI < 0.7, the phase values are set to zero as a masking procedure.

Prior to spatial interpolation and smoothing, the raw-phase difference map usually contains a linear variation along the radial direction, which is caused by any shift of refractivity over the entire map [refer to (7)]. This linear variation is calculated by averaging the slope (modulo-mapped) of all adjacent gate pairs that were previously masked in. Then, the estimated mean gradient is removed so that the raw-difference map is left with only the residual component, which wraps slower and is more readily processed for the subsequent interpolation and smoothing. As will be described in the next section, the linear gradient is added back after this quality control step.

Targets of interest are from near-stationary ground clutter and are limited in coverage and quality. As a result, the next step in the processing is a combined interpolation/smoothing procedure.

2) Spatial Interpolation and Smoothing of Raw Phase Difference Map: In our implementation, the phase difference map is first converted to a complex exponential form $\exp(j\phi)$, with values set to zero for regions with poor or nonexistent ground targets. Subsequently, the real and imaginary components are processed separately through an equivalent 2-D filtering (weight-and-sum) procedure in order to achieve the interpolation and smoothing. Smoothing using the complex exponential form, rather than direct phase measurements, avoids the abrupt phase wrapping and difficulties with smoothing over such transitions.

Spatial interpolation and smoothing are achieved using two distinct convolution processes. As radar data are acquired in a circular scanning manner, it is intuitive that one of the convolution processes would have a circular nature. Here, we chose the first to be the circular convolution using a Gaussian window running across azimuth angle of each range gate, followed by a second convolution across the range gates of each azimuth angle. The order of the operations is unimportant, since convolution is a linear operator. In essence, this simple two-step convolution produces a smoothed map that is the same as what would be produced using a 2-D Gaussian filter but is more computationally efficient.

For each of the convolution operations mentioned, the smoothing window is generated using the following three-step procedure.

Step 1) Initiate a K-tap Gaussian window as follows:

$$w''[k] = \exp\left[-2\left(\frac{k-(K-1)/2}{\sigma}\right)^2\right] \tag{10}$$

for $k = 0, 1, 2, \ldots, (K-1)$, where σ is the width of the smoothing window normalized to the sampling interval, i.e., $w''[k]$ is a K-sample wide window and is formulated as follows:

$$\sigma = \begin{cases} \frac{W}{r\Delta\theta}, & \text{for cross-azimuth smoothing} \\ \frac{W}{\Delta r}, & \text{for cross-range smoothing} \end{cases} \tag{11}$$

where W is the physical width and is usually set to 2.5 km. $r\Delta\theta$ is the arc length between radials at range r, and Δr is the range-gate separation.

Step 2) Truncate the smoothing window as follows:

$$w'[k] = \begin{cases} 0, & \text{for} \quad w''[k] < 10^{-3} \\ w''[k], & \text{otherwise} \end{cases} \tag{12}$$

where the threshold is arbitrary but is typically chosen to be small, e.g., 10^{-3}. The smoothing window is truncated so that no phase sample can have an effect at large spatial distance through the convolution process.

Step 3) Normalize the smoothing window for convolution as

$$w[k] = \frac{w'[k]}{\sum_{k=0}^{K-1} w'[k]}. \tag{13}$$

Note that the width of the smoothing window is range-dependent for cross-azimuth smoothing, since we desire to have an approximately constant physical width at all ranges. For a simple and efficient implementation, the smoothing window is initialized with $K = 359$ and then truncated as in (11).

The coefficients that were set to zero are tracked and ignored when applying the convolution operator. In other words, a shorter convolution window is used. By doing so, unnecessary computations used to multiply zero are eliminated, resulting in computational savings, particularly at large ranges. For cross-range smoothing, K is simply chosen to match the length at which it is to be truncated.

As a final step in the smoothing process, recall that the linear variation of phase as a function of range was removed in order to smooth only the perturbation component. At this point in the procedure, this deterministic linear-phase component is added back to the resulting smoothed phase.

3) Range Derivative: After the phase difference map is interpolated and smoothed, a radial derivative is derived by calculating the $\pm\pi$-modulo difference of the phase samples on a gate-to-gate basis. Therefore, (7) is applied as

$$\Delta N = -10^6 \frac{c}{4\pi f} \frac{\Delta}{\Delta r} \left[\phi(r, t_1) - \phi(r, t_0)\right]. \tag{14}$$

This term is expected to be noisy due to the mathematical characteristics of the derivative operator. In our experience, the standard deviation of this field can exceed 3 N units. Therefore, it is subsequently smoothed using the same two-step convolution process presented earlier. Absolute refractivity can be derived by adding the reference refractivity map to the difference, if desired.

4) Limitations of Refractivity Estimates: At a given discrete sampling interval in range (Δr), the accuracy of the derivative term is limited by how well the derivative is approximated by the finite difference in (14). As such, the maximum unambiguous estimate of the gradient of the phase difference term $\Delta[\phi(r, t_1) - \phi(r, t_0)]/\Delta r$ is limited to $\pm\pi/\Delta r$, which can be shown to have a maximum unambiguous refractivity difference of

$$\Delta N_a = \pm 10^6 \frac{c}{4f\Delta r}. \tag{15}$$

Recall that refractivity change is first estimated for its mean component, in which pairs of masked in-phase measurements are used, so the limit of mean refractivity change can be calculated from (15) once a particular radar configuration is realized. For the perturbation component of refractivity change (during smoothing), N_a becomes a function of local effective range-gate spacing (due to masking). In other words, the local limit is reduced to a fraction of (15), depending on the availability of ground targets. For other radar configurations, it should be noted from (15) that N_a can be improved by reducing Δr. This is important if the refractivity retrieval technique is to be applied to radars operating at higher frequencies, e.g., C- and X-band, in order to compensate for the limitations due to shorter wavelengths.

IV. First Results From the PAR

An experiment was conducted on September 28, 2005, using the NWRT PAR system for refractivity retrieval, when a 1-h time-series data set was collected at the lowest elevation angle (0.5°). During this time period, there was a strong low-level northerly wind of approximately 8 $\mathrm{m \cdot s^{-1}}$ causing a light dust storm with corresponding reflectivity values of 10–15 dBZ. With the strong wind and greater than 10 N-units spatial and temporal variations in the refractivity field (estimated through the Oklahoma Mesonet), a similar prominent change in the refractivity field from the PAR was expected.

A. Experimental Design

The PAR system was configured to perform continuous 90° sector scans over azimuth angles of $-45°$ to $+45°$. The PAR is set facing north in order to utilize the denser ground-target distribution, which is in between Norman and Oklahoma City. As mentioned before, the ground target useful for phase-change detection must be stationary. Therefore, targets like buildings and towers are useful, but trees are not appropriate for such application.

The broadside of the array was set to north and at an elevation angle of 0.5°, i.e., the lowest elevation angle allowed by the radar. It is emphasized here that the measurement height is a function of the target height but not the beam height. To be precise, the radar return is from the parts of the beam coincident with the clutter target rather than the entire volume of the beam coverage. In some instances, a return could come from a part of a sidelobe, but if there is no interference, the phase is still representative for refractivity retrieval. These characteristics are different from most weather-radar-like applications. A pertinent question is at what exact height and regions are the refractivity being measured. This question is currently unresolved and should be considered when comparing the radar refractivity with surface measurements. Another known and relatively easier problem is the terrain height in which the vertical component of refractivity can be removed using a mean refractivity profile, which is a function of terrain height [2]. However, this method is not applied here, since the terrain near Norman is relatively flat.

For the PAR system, no beam smearing would be expected, given this electronic-step-scanning strategy. The collection parameters were set to operate at a pulse repetition time (PRT) of 1 ms, and 64 consecutive I/Q samples were collected for each beam position. Given the operating frequency of 3.2 GHz, the resultant aliasing velocity is 23.4 $\mathrm{m \cdot s^{-1}}$. Including instrumental overhead, the collection parameters resulted in a temporal resolution of 5.76 s for the 64-pulse 90-position scans. In this experiment, phase and refractivity change fields at 19:00 UTC is set to be the reference.

B. Rapid Variations in Refractivity Fields

Refractivity field retrieved using the phase measurement from a radar can potentially have a very high temporal resolution. However, it must be emphasized that there are rapid fluctuations in the change of refractivity field particularly in regions with poor ground-clutter coverage. This is not surprising, since refractivity field is obtained through the radial derivative of phase measurements [refer to (7)], which can produce increased statistical uncertainty.

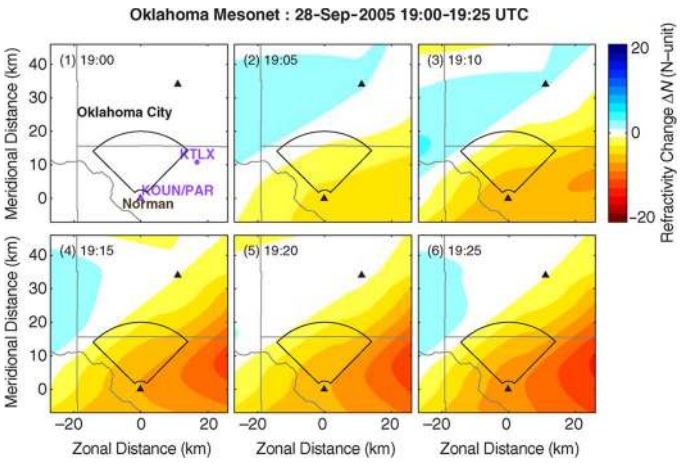

Fig. 6. Refractivity change fields derived from surface measurements of the Oklahoma Mesonet, which serve as ground truth for the validation of refractivity retrieval using the NWRT PAR. The reference time is at 19:00 UTC. The solid 90° sector polygon indicates the area of interest for the PAR–Mesonet comparison and the solid triangles indicate the positions of the Mesonet stations and the radar at the origin.

Oklahoma enjoys the benefits of a reliable high-quality network of surface stations, known as the Oklahoma Mesonet, which was developed jointly by the Oklahoma State University and OU [21], [22]. The Oklahoma Mesonet is a unique surface network that measures environmental conditions such as wind speed and direction, air temperature, barometric pressure, and air relative humidity. These measurements are acquired with 5-min temporal resolution, and the data are accessible in real-time through a reliable web portal. There are more than 110 stations in the Oklahoma Mesonet that are currently in operation [22], [23]. The average spacing between adjacent Mesonet stations is approximately 35 km. Under conditions where the spatial structure of refractivity is not complex, the Oklahoma Mesonet allows for the derivation of an accurate reference refractivity map via (2) and 2-D objective analysis.

A sequence of images of refractivity change from the Oklahoma Mesonet is shown in Fig. 6, with a similar plot from the PAR measurements shown in Fig. 7. More images are available (every 5.76 s), but only a subset is shown here. As aforementioned, the temporal resolution of the measurements from the Oklahoma Mesonet is 5 min, which is the same temporal spacing between adjacent images in the leftmost column of Fig. 7.

From this comparison between the PAR and the Oklahoma Mesonet, we have qualitatively established the validation of refractivity retrieval with surface measurements. It can be seen that refractivity field is estimated with reasonable accuracy by applying the retrieval algorithm to the S-band PAR. In the next section, rapid scanning using the PAR will be discussed by exploiting the agile beam-steering capability of this electronic scanning system.

V. Potential for Multimission Refractivity Surveillance

An MPAR is a radar concept system that can simultaneously be tasked for aircraft tracking and weather surveillance [17]. With a single radar system that performs multiple tasks, a reduction in maintenance and logistic infrastructure costs can be realized. An MPAR system would utilize an electronic-scanning mechanism to rapidly steer the beam. With this agile beam-steering capability, the radar could probe several regions by time sharing the tasks, e.g., aircraft tracking and weather observations. In addition, the beam-steering agility could be exploited to minimize volume-scan update time using a beam-multiplexed scanning approach [24]. By rapidly scanning spatially separated positions and resampling only after sufficient time for signal decorrelation has elapsed, more statistically robust moment estimation can be obtained.

In this section, the refractivity fields (derived from 64-pulse dwell) will be used as ground truth for the comparison. Subsets of contiguous pulses will be extracted from each scan to emulate refractivity fields derived from shorter dwells, which represent faster scans. The goal is to investigate refractivity estimates from extremely short dwell times. It must be emphasized here that theoretical analysis of the error for the algorithm would be difficult, given the complex and nonlinear steps (refer to Section III) involved in the retrieval algorithm. In lieu of this analysis, real data are used to systematically study the effect of short dwell times on system performance. Here, 32-, 16-, 8-, 4-, and 2-pulse dwells will be tested and compared against the reference (64-pulse dwell). A one-sample dwell was not tested, because radial-velocity estimation would not be possible and is a key component for the determination of the quality of ground targets. An example of such a comparison is shown in Fig. 8, where the number of pulses is indicated in the upper left corner.

Recall from Section III that the phase difference map was spatially interpolated and smoothed with phase converted into the complex form $\exp(j\phi)$. While the phase of the interpolated-and-smoothed map is used for refractivity calculation, the magnitude is used as our quality metric for refractivity field partitioning. The magnitude is mapped into a censoring index (CI) as follows:

$$\mathrm{CI} = 1 - 0.25 \log_2 \left(1 - \log_{10}(M)\right) \tag{16}$$

where M represents the magnitude of the interpolated-and-smoothed phase samples. Since the phase samples are in $\exp(j\phi)$ form and the smoothing windows are magnitude normalized $M \leq 1$, CI is limited to a maximum of unity. For our statistical comparisons, three partitions have been created to represent regions with high, mid, and low quality of estimates. The three regions have CI as follows:

$$\text{Region quality} = \begin{cases} \text{high}, & 0.6 < \mathrm{CI} \leq 1.0 \\ \text{mid}, & 0.5 < \mathrm{CI} \leq 0.6 \\ \text{low}, & 0.4 < \mathrm{CI} \leq 0.5 \\ \text{censored}, & \mathrm{CI} \leq 0.4. \end{cases} \tag{17}$$

From Fig. 8, note that maps of refractivity change derived from various number of pulses appear qualitatively similar, providing promise that extremely short dwell times are possible. For a statistical comparison, different quality of refractivity fields are partitioned and extracted for performance evaluation. A plot of the root-mean-squared (rms) error (using the 64-point

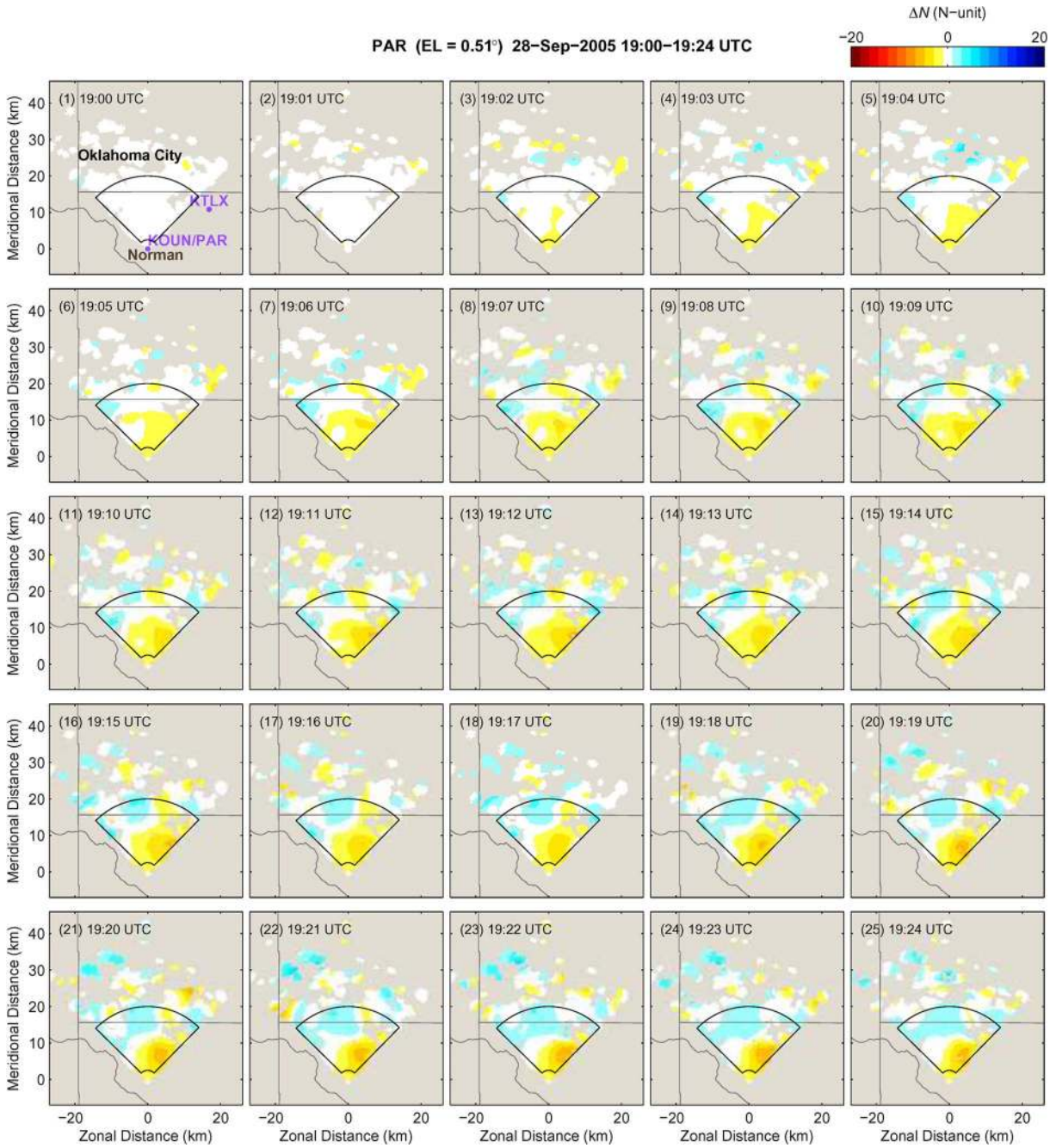

Fig. 7. Time history of the refractivity change field retrieved using the PAR measurements shows similar spatial and temporal change from the refractivity fields derived from the Oklahoma Mesonet. During this 25-min period, one can see an increase in the refractivity field in the northwestern region but a decrease in the region nearer the radar.

dwell as the reference) for various number of samples is shown in Fig. 9. As one would expect, for a particular number of samples, the rms error increases as the quality metric decreases. Furthermore, as the number of samples increases toward 64, the rms error decreases. Note that for a two-sample dwell time, the rms error, and its standard deviation are approximately one N unit and less than one N unit, respectively. This performance is despite the relatively low-quality data resulting from the dust storm. An explanation for this exceptional performance is that the SNR of the ground targets is sufficiently high. SNR values of 40–60 dB can be found within the coverage area and represent the particular targets used for the extraction of refractivity retrieval. As such, even a two-sample dwell time (with spatial smoothing) suffices for the necessary phase measurements. This two-sample dwell with a PRT of 1 ms translates into an extremely rapid 180-ms scan time for a 90° coverage using the PAR.

For consistency, another independent data set was analyzed with the error calculations briefly presented here. The experimental design was identical to the previous case, but the meteorological conditions were clear without contamination due to the dust storm. For the refractivity field, there was no significant spatial variation within the field of view. Nonetheless, there was a general trend of refractivity change that was used in

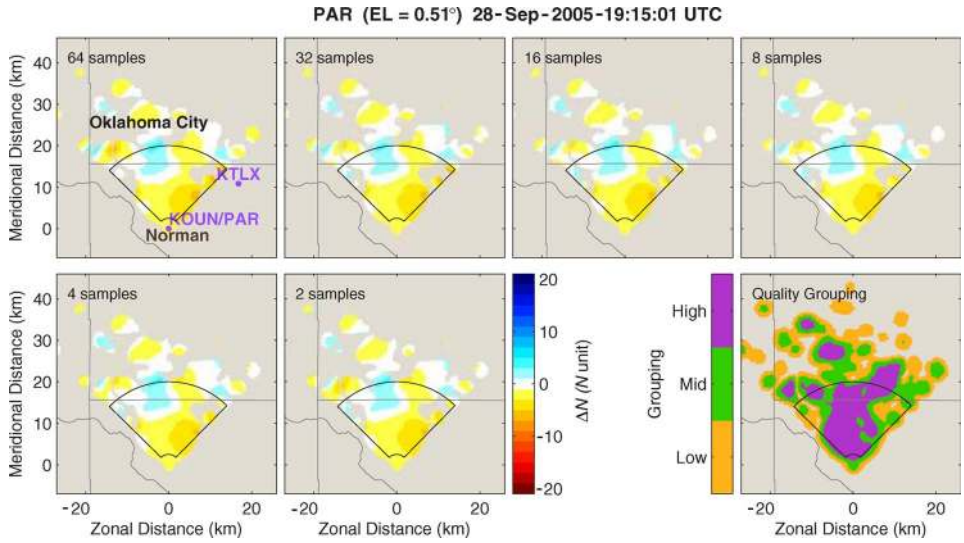

Fig. 8. Comparison of refractivity changed derived from different number of samples. Similar fields show the potential of rapid retrieval with the PAR system. Using the weight-and-sum phase values within the smoothing window, the resulting magnitude is used as a metric to indicate the quality of the derived field. Here, the field is partitioned into three regions with different QIs (high, mid, and low) for comparison.

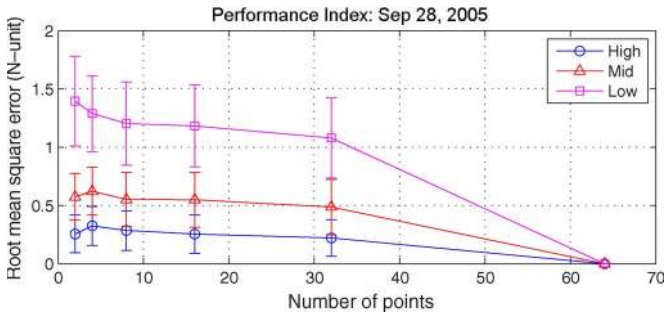

Fig. 9. RMS error from refractivity fields retrieved for various dwell times using the 64-sample case as the reference. The error is calculated over the three different regions indicated in Fig. 8 for different quality levels.

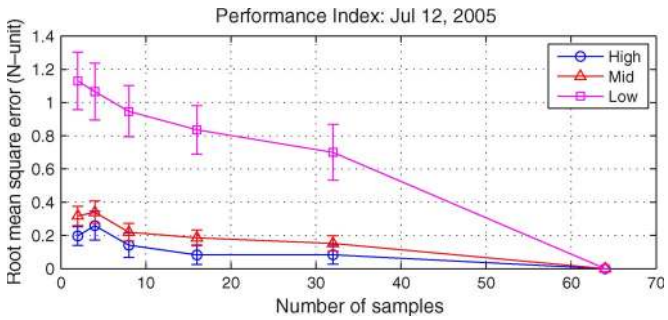

Fig. 10. Same as Fig. 9 except for data from July 12, 2005. RMS error was lower as expected, given the comparatively clear conditions.

comparison to surface measurements from the Oklahoma Mesonet. A similar behavior of the rms error as in the previous example is shown in Fig. 10. Without dust interference, the performance of the two-sample dwell is improved with rms error less than 0.4 N units for the mid-quality level.

In this section, it has been shown that statistically significant refractivity fields can be retrieved rapidly with as few as two pulses. To put this result in the context of the MPAR concept, refractivity retrieval can be added to the total operation by steering the beam to the lowest elevation angle for a set of 180 pulses for every volume scan. Therefore, this rapid refractivity retrieval would put only a minimum resource burden on the other missions of a future MPAR system.

VI. Conclusion

It has been shown that refractivity retrieval is viable using phase measurements from the S-band PAR of the NWRT. The refractivity fields were compared and validated with surface measurements from the Oklahoma Mesonet and were found to be in good agreement. Subsets of the raw samples from the PAR system were extracted to emulate shorter dwell times. From this procedure, it has been shown that refractivity retrieval can be accomplished successfully with as little as two samples. If the MPAR system is to become a reality, rapid refractivity retrieval is certainly attractive and would add an important capability to the system. Future plans include simulation studies for quantitative-error analyses for the refractivity retrieval technique under varying meteorological conditions.

References

[1] F. Fabry, C. Frush, I. Zawadzki, and A. Kilambi, "On the extraction of near-surface index of refraction using radar phase measurements from ground targets," *J. Atmos. Ocean. Technol.*, vol. 14, no. 4, pp. 978–987, Aug. 1997.

[2] F. Fabry, "Meteorological value of ground target measurements by radar," *J. Atmos. Ocean. Technol.*, vol. 21, no. 4, pp. 560–573, Apr. 2004.

[3] W. F. Dabberdt and T. W. Schlatter, "Research opportunities from emerging atmospheric observing and modeling capabilities," *Bull. Amer. Meteorol. Soc.*, vol. 77, no. 2, pp. 305–323, Feb. 1996.

[4] S. E. Koch, A. Aksakal, and J. T. McQueen, "The influence of mesoscale humidity and evapotranspiration fields on a model forecast of a cold-frontal squall line," *Mon. Weather Rev.*, vol. 125, no. 3, pp. 384–409, Mar. 1997.

[5] N. A. Crook, "Sensitivity of moist convection forced by boundary layer processes to low-level thermodynamic fields," *Mon. Weather Rev.*, vol. 124, no. 8, pp. 1767–1785, Aug. 1996.

[6] T. M. Weckwerth, J. W. Wilson, and R. M. Wakimoto, "Thermodynamic variability within the convective boundary layer due to horizontal convective rolls," *Mon. Weather Rev.*, vol. 124, no. 5, pp. 769–784, May 1996.

[7] C. L. Ziegler, T. J. Lee, and R. A. Pielke, Sr., "Convective initiation at the dryline: A modeling study," *Mon. Weather Rev.*, vol. 125, no. 6, pp. 1001–1026, Jun. 1997.

[8] C. L. Ziegler and E. N. Rasmussen, "The initiation of moist convection at the dryline: Forecasting issues from a case study perspective," *Weather Forecast.*, vol. 13, no. 4, pp. 1106–1131, Dec. 1998.
[9] D. B. Parsons, M. A. Shapiro, and E. Miller, "The mesoscale structure of a nocturnal dryline and of a frontal–dryline merger," *Mon. Weather Rev.*, vol. 128, no. 11, pp. 3824–3838, Nov. 2000.
[10] Y.-R. Guo, Y.-H. Kuo, J. Dudhia, D. Parsons, and C. Rocken, "Four-dimensional variational data assimilation of heterogeneous mesoscale observations for a strong convective case," *Mon. Weather Rev.*, vol. 128, no. 3, pp. 619–643, Mar. 2000.
[11] T. M. Weckwerth and D. B. Parsons, "An overview of the International H_2O Project (IHOP_2002)," *Bull. Amer. Meteorol. Soc.*, vol. 85, no. 2, pp. 253–277, 2003.
[12] B. L. Cheong, R. D. Palmer, C. D. Curtis, T.-Y. Yu, D. Zrnić, and D. Forsyth, "Refractivity measurements from ground clutter using the national weather radar testbed phased array radar," in *Proc. 32nd Conf. Radar Meteorol.*, Oct. 2005. CD-ROM P1R10.
[13] J. A. Brotzge, K. Brewster, B. Johnson, B. Philips, M. Preston, D. Westbrook, and M. Zink, "CASA's first testbed: Integrated Project #1 (IP1)," in *Proc. 32nd Conf. Radar Meteorol.*, 2005. CD-ROM 14R.2.
[14] R. D. Palmer, B. L. Cheong, K. Hardwick, P. S. Tsai, S. J. Frasier, B. Bowie, P. Kennedy, D. Brunkow, and V. Chandrasekar, "Refractivity retrieval using X-band radars: Mitigation of rapid phase wrapping," in *Proc. PIERS*, Tokyo, Japan, Aug. 2–5, 2006.
[15] B. L. Cheong, K. Hardwick, J. Fritz, P. S. Tsai, R. D. Palmer, V. Chandrasekar, S. J. Frasier, J. George, D. Brunkow, B. Bowie, and P. Kennedy, "Refractivity retrieval using the CASA X-band radars," in *Proc. 33rd Conf. Radar Meteorol.*, Aug. 2007, p. P8B.9.
[16] D. E. Forsyth, J. F. Kimpel, D. S. Zrnić, R. Ferek, J. F. Heimmer, T. McNellis, J. E. Crain, A. M. Shapiro, R. J. Vogt, and W. Benner, "The national weather radar testbed (Phased Array)," in *Proc. 32nd Conf. Radar Meteorol.*, 2005. CD-ROM 12R.3.
[17] M. Weber, J. Cho, J. Flavin, J. Herd, and M. Vai, "Multi-function phased array radar for U.S. civil-sector surveillance needs," in *Proc. 32nd Conf. Radar Meteorol.*, Oct. 2005, pp. 24–29.
[18] J. Sensi, Jr., "The AEGIS system," in *Aspects of Modern Radars*. Norwood, MA: Artech House, 1988, pp. 239–277.
[19] D. S. Zrnić, J. F. Kimpel, D. E. Forsyth, A. Shapiro, G. Crain, R. Ferek, J. Heimmer, W. Benner, T. J. McNellis, and R. J. Vogt, "Agile beam phased array radar for weather observations," *Bull. Amer. Meteorol. Soc.*, vol. 88, no. 11, pp. 1753–1766, Nov. 2007.
[20] B. R. Bean and E. J. Dutton, *Radio Meteorology*. New York: Dover, 1968.
[21] F. V. Brock, K. C. Crawford, R. L. Elliott, G. W. Cuperus, S. J. Stadler, H. L. Johnson, and M. D. Eilts, "The Oklahoma Mesonet: A technical overview," *J. Atmos. Ocean. Technol.*, vol. 12, no. 1, pp. 5–19, Feb. 1995.
[22] R. A. McPherson, C. A. Fiebrich, K. C. Crawford, R. L. Elliott, J. R. Kilby, D. L. Grimsley, J. E. Martinez, J. B. Basara, B. G. Illston, D. A. Morris, K. A. Kloesel, S. J. Stadler, A. D. Melvin, A. J. Sutherland, H. Shrivastava, J. D. Carlson, J. M. Wolfinbarger, J. P. Bostic, and D. B. Demko, "Statewide monitoring of the mesoscale environment: A technical update on the Oklahoma Mesonet," *J. Atmos. Ocean. Technol.*, vol. 24, no. 3, pp. 301–321, Mar. 2007.
[23] C. A. Fiebrich, D. L. Grimsley, R. A. McPherson, K. A. Kesler, and G. R. Essenberg, "The value of routine site visits in managing and maintaining quality data from the Oklahoma Mesonet," *J. Atmos. Ocean. Technol.*, vol. 23, no. 3, pp. 406–416, Mar. 2006.
[24] M. B. Orescanin, T.-Y. Yu, C. D. Curtis, D. S. Zrnić, and D. Forsyth, "Signal processing of beam-mutiplexed data for phased-array weather radar," in *Proc. 32nd Conf. Radar Meteorol.*, 2005. CD-ROM 4R.6.

Boon Leng Cheong received the B.S.E.E., M.S.E.E., and Ph.D. degrees in electrical engineering from the University of Nebraska, Lincoln, in 1999, 2002, and 2005, respectively.

Since 2005, he has been a Postdoctoral Fellow with the School of Meteorology, University of Oklahoma, Norman. Besides work on refractivity retrieval, his research interests include numerical radar simulations, array processing using multiple receivers, and real-time signal processing applied to radar and acoustic applications. Recently, he has developed a radar time-series simulator that utilizes realistic atmospheric fields.

Robert D. Palmer received the Ph.D. degree in electrical engineering from the University of Oklahoma, Norman.

From 1989 to 1991, he was a Postdoctoral Fellow with the Radio Atmospheric Science Center, Kyoto University, Kyoto, Japan, where his major accomplishments were the development of novel interferometric radar techniques for studies of the lower and middle atmosphere. From 1993 to 2004, he was a Member of the Faculty with the Department of Electrical Engineering, University of Nebraska, Lincoln, where his interests broadened into areas including wireless communications, remote sensing, and pedagogy. He was a Research Associate with the Physics and Astronomy Department, Clemson University, Clemson, SC, where he continued his work with atmospheric radar. He is currently the Tommy C. Craighead Chair with the School of Meteorology, University of Oklahoma (OU), Norman, where he is also an Adjunct Professor with the School of Electrical and Computer Engineering. He is also currently leading OU's interdisciplinary Atmospheric Radar Research Center, which is the focal point for the weather radar research and educational activities on the Norman campus. Since coming to OU, his research interests have been focused primarily on the application of advanced radar signal processing techniques to observations of severe weather, particularly related to phased-array radars and other innovative system designs. He has published widely in the area of radar remote sensing of the atmosphere, with an emphasis on generalized imaging problems, spatial filter design, and clutter mitigation using advanced array/signal processing techniques.

Dr. Palmer was the recipient of several awards for both his teaching and research accomplishments while in the University of Nebraska.

Christopher D. Curtis received the B.S. degree in mathematics from the University of Oklahoma, Norman, in 1992 and the M.S. degree in applied mathematics from the University of Illinois at Urbana–Champaign, Urbana, in 1993.

From 1995 to 1999, he was with the Radar Signal Processing Group, Texas Instruments. He was then with Raytheon, Plano, TX. He is currently with the Cooperative Institute for Mesoscale Meteorological Studies, University of Oklahoma, which is affiliated with the National Severe Storms Laboratory, National Oceanic and Atmospheric Administrations/OAR, Norman. His research interests include the area of signal processing with applications to phased-array and Doppler weather radars.

Mr. Curtis is a member of Phi Beta Kappa.

Tian-You Yu received the B.S. degree in atmospheric physics and the M.S. degree in space science from the National Central University, Taoyuan, Taiwan, R.O.C., and the Ph.D. degree in electrical engineering from the University of Nebraska, Lincoln, in 2000.

He was a Postdoctoral Fellow with the National Center for Atmospheric Research. He had worked on various types of profiler radars to study atmospheric dynamics from the boundary layer to the mesosphere. He is currently an Assistant Professor with the School of Electrical and Computer Engineering, University of Oklahoma, Norman. He has a wide range of interests that include digital signal processing and atmospheric applications through radar observations. His current interest includes the development of novel and sophisticated radar technologies to improve radar measurement and the advancement of the fundamental knowledge of meteorological phenomena.

Dusan S. Zrnić was born in Belgrade, Yugoslavia, on June 3, 1942. He received the Dipl.Ing. degree in electrical engineering from the University of Belgrade, Belgrade, Serbia, in 1965 and the M.Sc. and Ph.D. degrees in electrical engineering from the University of Illinois at Urbana–Champaign, Urbana, in 1965.

He was a Research and Teaching Assistant with the Charged Particle Research Laboratory, University of Illinois at Urbana–Champaign. He was with the Electrical Engineering Department, California State University, Northridge, where he was an Associate Professor in 1974 and a Professor in 1978. From 1973 to 1974, he was a National Research Council Postdoctoral Fellow with the National Severe Storms Laboratory, National Oceanic and Atmospheric Administrations (NOAA)/OAR, Norman, where he is currently the Leader of the Doppler Radar and Remote Sensing Research Group. He is currently also an Adjunct Professor of electrical engineering and meteorology with the University of Oklahoma, Norman. His research experience includes circuit design, applied mathematics, magnetohydrodynamics, radar signal processing, and systems design. Recently, he has spent considerable effort toward improvements of weather radar signal processing, advancements of polarimetric measurements and their interpretation, and development of algorithms for NEXRAD. He has published extensively on weather radar signal processing, radar meteorology, and remote sensing. The most important and representative publication is the book *Doppler Radar and Weather Observations* (Academic Press, 1984, second edition 1993, coauthored with Dr. Richard Doviak). He is the holder of three U.S. patents in the area of weather radar technology.

Dr. Zrnić has been a member of URSI Commissions C and F. He is a Fellow of the AMS. He was the recipient of three Best Research Paper Awards form NOAA's Office of Ocean and Atmospheric Research. He was the corecipient of the IEEE 1988 Harry Diamond Memorial Award for contributions to and applications of weather radar science and was also the corecipient of the 1993 IEEE Donald G. Fink Prize Award with Dr. P. Mahapatra. He was the corecipient with R. V. Ryzhkov of the WMO 1996 Vaisala Award. In 2004, he was the recipient of the Presidential Rank Award for exceptional long-term accomplishments. In 2006, he was elected to the U.S. National Academy of Engineering with the citation: For development of potent radar methods that have greatly enhanced operational weather detection and warning and advanced meteorological research.

Douglas Forsyth was born in Watertown, SD. He received the B.S. degree in electrical engineering from South Dakota State University, Brookings, in 1971, the B.S. degree in meteorology from Pennsylvania State University, University Park, in 1972, and the M.S. degree in meteorology from the University of Oklahoma, Norman, in 1979.

After spending 14 years in the Air Force, he has been with the National Severe Storms Laboratory, National Oceanic and Atmospheric Administrations (NOAA)/OAR, Norman, since 1985, where he has served as Interim Director, Deputy Director, Assistant Director, Manager of two divisions, and Manager of Special Projects. In 2000, he completed a temporary assignment with NOAA headquarters as Acting Director of the Information Systems Office and Chief Information Officer of NOAA. Since 1995, has been serving as the NOAA Program Manager for construction of the National Weather Center. He also leads the Radar Research and Development Division, a group of 40 professionals working on radar improvements such as dual-polarization and phased-array radar. His background is in radar meteorology, radar algorithm development, and project and facility management. He participated in the Joint Doppler Operational Project that led to implementation of Doppler radars across this nation. He wrote some of the first radar algorithms used to process radar data in real-time and is currently a member of the NEXRAD Technical Advisory Committee. In 1997, he was named the Oceanic and Atmospheric Research (OAR) Employee of the Year. He completed the Senior Executive Fellows program at the JFK School of Government, Harvard University in 1992 and NOAAs Leadership Competencies Development program in 2000.

Dr. Forsyth is a member of the American Meteorological Society, National Weather Association, and American Radio Relay League. As an active volunteer, he has served the United Way of Norman on the Campaign Cabinet from 1995 to 1998, on the Board of Directors from 1999 to 2005, and as Board President in 2003. In 2007, he was the recipient of the NOAA Administrators Award for his leadership in overseeing the design, construction, and occupancy of the National Weather Center, a joint NOAA and University of Oklahoma project. In addition, he has served on Norman's 2025 Land Use and Transportation Planning Committee and Committee to End Chronic Homeless. He is currently the Cochair of the oversight committee to End Chronic Homelessness. In addition, he is currently leading an effort to build a weather museum in Norman, OK.